coatings MDPI

Article

The Local Distribution of Temperatures and Entropy Generation Rate in an Ideal Counterflow Heat Exchanger

Zhimin Dong * **and Qinglin Du**

School of Energy and Power Engineering, Huazhong University of Science and Technology, Wuhan 430074, China; qinglin_du@hust.edu.cn
* Correspondence: dongzhimin@hust.edu.cn

Abstract: The process of heat exchange between two fluids of different temperatures and separated by a solid wall occurs in many engineering applications. Log mean temperature difference and effectiveness-*NTU* methods are widely used to assist in the design of heat exchangers. However, the two methods focus on overall analysis and cannot show the local temperature distributions. This paper obtains the mathematical solutions to the temperature profiles in an ideal counterflow heat exchanger. The aim of this research is to explain the phenomenon called the "entropy generation paradox", which indicates a discrepancy between effectiveness and optimal entropy generation. The theoretical analysis reveals that the temperature curves are exponential functions when the heat capacity rates of the two streams are different; otherwise, the curves are linear functions. A heat exchanger is demonstrated to draw the temperature profiles under different working conditions. Local entropy generation rates are determined by the ratio of local stream temperatures in the form of a hook function. To realize a certain heat duty, there are many stream flow rate couples, and each couple results in a different entropy generation profile and obtains a corresponding total entropy generation. The helical steam generator of a high-temperature gas-cooled reactor is analyzed in this article and the principle of equipartition of entropy generation is confirmed. This principle indicates that, among the many working conditions to achieve a certain heat duty, a heat exchanger characterized by a nearly constant entropy production gives the best second law efficiency possible in order to achieve the best energy conversion.

Keywords: heat exchanger; mathematical solution; temperature profile; entropy generation; irreversibility

Citation: Dong, Z.; Du, Q. The Local Distribution of Temperatures and Entropy Generation Rate in an Ideal Counterflow Heat Exchanger. *Coatings* **2021**, *11*, 970. https://doi.org/10.3390/coatings11080970

Received: 14 July 2021
Accepted: 13 August 2021
Published: 15 August 2021

1. Introduction

The specific applications of heat exchangers may be found in space heating, air-conditioning, power production, waste heat recovery, and chemical processing. The most common arrangements for flow paths within a heat exchanger are counterflow and parallel flow. The counterflow heat exchanger, which is usually abbreviated to CFHX, has three significant advantages over the parallel flow design. First, the more uniform temperature difference between the two fluids minimizes the thermal stresses throughout the exchanger. Second, the outlet temperature of the cold fluid can approach the highest temperature of the hot fluid. Third, the more uniform temperature difference produces a more uniform rate of heat transfer throughout the heat exchanger.

Researchers have proposed a wide variety of heat exchangers to improve industry efficiency. Arani used a combined baffle and longitudinal ribbed tube configuration to optimize the fluid flow and heat transfer of water inside a segmental baffle shell and tube heat exchanger, the performance evaluation criterion of which was improved by 13–39% [1]. Chekurov demonstrated the effect of additive manufacturing design on the CFHX, showing that the novel structure improved the performance of the heat transfer process [2]. Phase change materials are used in thermal energy storage and, along with the physical properties of the materials, the performance of a latent heat-based thermal energy storage system depends on the design of the heat exchanger [3]. Sheikholeslami induced nanoparticles into the working fluids of the discharging system. Fins were employed, too. The discharging rate of the phase change material in the heat exchanger was improved significantly [4]. El-Said experimentally investigated four heat exchangers with different segmental baffle configurations, which were conventional single segmental baffle, staggered single segmental baffle, flower segmental baffle and hybrid segmental baffle. The new configurations improved the performance of the heat exchangers and the hybrid segmental baffle performed best, enhancing the energy efficiency by 1.27 to 1.4 times [5]. On the tube site, a kind of helical screw tape was investigated numerically according to the principle of heat transfer enhancement in the core flow of tube, making the temperature uniform and reducing the flow resistance [6]. The concept of physical quantity synergy was proposed as a guide to reveal the mechanism of heat transfer enhancement and flow character. The angle between the temperature gradient and velocity reflects heat transfer performance, while that between pressure gradient and velocity reflects flow resistance [7,8]. An experiment based on field synergy was carried out to analyze the thermal and flow characteristics in a circular tube [9]. Furthermore, exergy destruction was treated as a criterion to optimize the heat transfer activities [10]. As a result of the optimization, multi-longitudinal vortex generators have been employed to improve the performance of heat transfer, and many enhancement techniques are introduced in the review in [11].

In most industrial applications, computational fluid dynamics technology is widely used to design and optimize heat exchangers, avoiding numerous expensive experimental tests [12]. Theoretically, the logarithmic mean temperature difference method is useful to design and predict the performance of a CFHX,

$$Q = hA\frac{\Delta T_A - \Delta T_B}{\ln \Delta T_A - \ln \Delta T_B}$$

where ΔT_A is the temperature difference between the two streams at end A, and ΔT_B is the temperature difference between the two streams at end B. While, in a real industry design, the outlet temperatures may be not known and require iterations, in these cases and in some others, the effectiveness-*NTU* method will be used instead:

$$Q = \varepsilon C_{min}(t_{hin} - t_{cin})$$

where C_{min} is the minimum heat capacity rate of the streams

$$\varepsilon = \frac{1 - \exp\left(-NTU\left(1 - \frac{C_{min}}{C_{max}}\right)\right)}{1 - \frac{C_{min}}{C_{max}}\exp\left(-NTU\left(1 - \frac{C_{min}}{C_{max}}\right)\right)}$$

and

$$NTU = \frac{hA}{C_{min}}$$

When $C_{min} = C_{max}$,

$$\varepsilon = \frac{NTU}{1 + NTU}$$

Prof. Bergman revealed the derivative of the above relationship between ε, *NTU* and C_r in the eleventh chapter of his textbook [13]. The ε-*NTU* method is used widely in heat exchanger design. The effects of operational and geometrical parameters on the thermal effectiveness of shell and helically coiled tube heat exchangers ware investigated through numerical methods and experimental validation. For the same values of *NTU* and C_r, the effectiveness of shell and coiled tube heat exchangers was on average 12.6% less than the effectiveness of the parallel flow heat exchangers and this difference was approximately constant [14].

However, the ε-NTU method is based on overall analysis. It does not give the local temperature distributions and thus is not able to identify the features of a counterflow heat exchanger. This article obtains the temperature profiles in an ideal CFHX and analyzes the features of them.

Prof. Bejan outlined the method of entropy generation minimization to realize thermodynamic optimization:

$$\begin{aligned}\dot{S}'_{gen} &= \dot{S}'_{gen,\Delta T} + \dot{S}'_{gen,\Delta P} \\ &= \frac{q'\Delta T}{T^2} + \frac{\dot{m}}{\rho T}\left(-\frac{\mathrm{d}P}{\mathrm{d}x}\right)\end{aligned}$$

where $\dot{S}'_{gen,\Delta T}$ represents the entropy generation contributed by heat transfer, and $\dot{S}'_{gen,\Delta P}$ represents that contributed by flow resistance [15]. In many systems, the various mechanisms and design features that account for irreversibility compete with one another. For this reason, the thermodynamic optimum is the condition of the most advantageous trade-off between two or more competing irreversibilities. Each attempt in augmenting the overall heat transfer coefficient is accompanied by an increase in the pressure drop. Moreover, the minimization of entropy generation in many processes was investigated by Prof. Bejan and the studies are described in [16]. Nummedal stated that, in order to achieve the same heat duty with minimum entropy generation in a heat exchanger, the difference in inverse temperatures must be constant at minimal entropy production throughout the entire heat exchanger. This result is called the principle of equipartition of forces, and the deviation is very small [17].

Nanofluid with CuO nanoparticles was used to improve the performance of a heat exchanger, and this technique was combined with a swirl flow generator. Minimizing entropy generation was considered as the main aim to optimize the parameters of the nanofluid and turbulator [18]. In another study, entropy generation and forced convection heat transfer of Al_2O_3-water nanofluid in a heat exchanger equipped with helical twisted tape was investigated via a finite volume method [19]. Five different shapes of boehmite alumina nanoparticles, i.e., cylindrical, brick, blade, platelet and spherical, were compared. The research revealed that nanofluids containing cylindrical-shaped nanoparticles and nanofluids with platelet-shaped nanoparticles had the highest and lowest thermal conductivity, respectively [20]. Lerou treated the total heat leakage as a part of the production of entropy in a heat exchanger that was employed for a recuperative cooling system. The treatment was convenient for comparing the irreversibilities in optimizing the design parameters [21]. Entropy generation in a counterflow gas to gas heat exchanger was analyzed and a new equation was adopted to express the entropy generation values for an imbalanced heat exchanger of similar design with the smallest deviation from the exact value [22].

Shah illustrated that the heat exchanger effectiveness can be maximized with an intermediate value or minimum at the maximum irreversibility operation point depending on the flow arrangement of the two streams [23]. This phenomenon has not been explained before, but in this paper, local entropy generation was obtained and used to reveal novel findings. Rauch gave an analytical dimensionless analysis of entropy generation and its ratio with the local exchanged heat flow rate for heat exchangers in which one of the streams condenses or evaporates [24]. This paper will present the local entropy generation rates using the temperature curves obtained and the features of the distribution will be analyzed in detail.

2. Temperature Distributions

When the working fluids flow through a heat exchanger, both streams consume mechanical energy due to the friction force. In reality, the objective of researchers is to design a certain counterflow heat exchanger to accommodate the transfer of a certain amount of heat between two fluids at given flow rates and inlet temperatures with specified amounts of pumping power for each stream.

A simplified schematic diagram of a counterflow heat exchanger is shown in Figure 1. The real heat exchange process is very complex, where the physical parameters of the working fluids have non-linear relations with temperature, which varies in the different parts of every cross-section, and so on. It is impossible to obtain a purely mathematical solution to a real heat exchange process. In this paper, some conditions are simplified as follows:

1. ignoring the temperature difference inside one stream at every cross-section;
2. the thermal parameters of the streams are independent of the temperature; if not, mathematical solutions can never be obtained due to the non-linearity of the equations;
3. there is no condensation or evaporation happening in the heat exchanger;
4. both streams are considered incompressible fluids;
5. the convection heat transfer coefficient is an inherent property of the heat exchanger and it will not change with different heat capacity rates of the two streams.

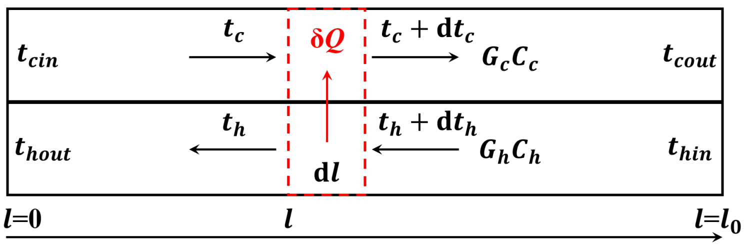

Figure 1. Schematic diagram of a counterflow heat exchanger.

At the place marked as ℓ, a finite volume having a length of $\mathrm{d}\ell$ contains two streams of working fluid whose respective mean temperatures are:

$$\overline{t_c} = \frac{t_c + (t_c + \mathrm{d}t_c)}{2}$$
$$\overline{t_h} = \frac{t_h + (t_h + \mathrm{d}t_h)}{2}$$

Thus, the heat transferred from the hot stream to the cold stream in the finite volume can be calculated as:

$$\begin{aligned}\delta Q &= h(\overline{t_h} - \overline{t_c}) \times A\,\mathrm{d}\ell \\ &= Ah\,\mathrm{d}\ell\left(t_h - t_c + \frac{\mathrm{d}t_h - \mathrm{d}t_c}{2}\right)\end{aligned} \tag{1}$$

where h is the convection heat transfer coefficient and A is the heat exchange area per unit length. In the meantime, according to the energy conservation law, δQ also represents the heat energy that the hot stream loses or the cold stream gains when they flow through the control volume, and it can be expressed by the following equations:

$$\delta Q = G_hC_h(t_h + \mathrm{d}t_h - t_h) = G_hC_h\,\mathrm{d}t_h \tag{2a}$$
$$\delta Q = G_cC_c(t_c + \mathrm{d}t_c - t_c) = G_cC_c\,\mathrm{d}t_c \tag{2b}$$

where G represents the mass flow rate and C represents the specific heat capacity at constant volume or constant pressure. G_hC_h and G_cC_c are the heat capacity rates of the hot stream and the cold stream, respectively.

With the simultaneous equations, Equation (2a,2b) rearranged with Equation (1), the infinitesimal increments can be ignored and the following equation can be obtained:

$$\frac{\delta Q}{\mathrm{d}\ell} = G_c C_c \frac{\mathrm{d}t_c}{\mathrm{d}\ell} = G_h C_h \frac{\mathrm{d}t_h}{\mathrm{d}\ell} = Ah(t_h - t_c) \tag{3}$$

This can be used to determine the temperature distributions of the two streams. The process can be summarized as follows: first of all, write the derivative of the differential equation, Equation (3), which is:

$$G_c C_c \frac{\mathrm{d}^2 t_c}{\mathrm{d}\ell^2} = G_h C_h \frac{\mathrm{d}^2 t_h}{\mathrm{d}\ell^2} = Ah\left(\frac{\mathrm{d}t_h}{\mathrm{d}\ell} - \frac{\mathrm{d}t_c}{\mathrm{d}\ell}\right) \tag{4}$$

Meanwhile, the relationship between $\frac{\mathrm{d}t_h}{\mathrm{d}\ell}$ and $\frac{\mathrm{d}t_c}{\mathrm{d}\ell}$ is clear from Equation (3):

$$\frac{\mathrm{d}t_h}{\mathrm{d}\ell} = \frac{G_c C_c}{G_h C_h} \frac{\mathrm{d}t_c}{\mathrm{d}\ell}$$

Then, replace the term $\frac{\mathrm{d}t_h}{\mathrm{d}\ell}$ in Equation (4) with $\frac{G_c C_c}{G_h C_h} \frac{\mathrm{d}t_c}{\mathrm{d}\ell}$; thus, the differential temperature equation for the cold stream is obtained as follows:

$$\frac{\mathrm{d}^2 t_c}{\mathrm{d}\ell^2} = Ah\left(\frac{1}{G_h C_h} - \frac{1}{G_c C_c}\right) \frac{\mathrm{d}t_c}{\mathrm{d}\ell}$$

the terms that are not associated with the t_h or t_c are marked as η to make the formula more concise:

$$\eta = Ah\left(\frac{1}{G_h C_h} - \frac{1}{G_c C_c}\right)$$

Similarly, the differential temperature equation for the hot stream is produced after the term $\frac{\mathrm{d}t_c}{\mathrm{d}\ell}$ in Equation (4) is replaced through the same method:

$$\frac{\mathrm{d}^2 t_c}{\mathrm{d}\ell^2} = \eta \frac{\mathrm{d}t_c}{\mathrm{d}\ell} \tag{5a}$$

$$\frac{\mathrm{d}^2 t_h}{\mathrm{d}\ell^2} = \eta \frac{\mathrm{d}t_h}{\mathrm{d}\ell} \tag{5b}$$

It is easy to obtain the general solutions to the above equations, Equation (5a,5b):

$$t_c = y\mathrm{e}^{\eta\ell} + x \tag{6a}$$

$$t_h = m\mathrm{e}^{\eta\ell} + n \tag{6b}$$

where x, y, m and n are arbitrary constants and can be confirmed by the boundary conditions, which are as follows: when ℓ is 0, $t_c = t_{cin}$ and at the place $\ell = \ell_0$, $t_h = t_{hin}$,

$$t_{cin} = y + x \tag{7a}$$

$$t_{hin} = m\mathrm{e}^{\eta\ell_0} + n \tag{7b}$$

Hence,

$$x = t_{cin} - y$$

$$n = t_{hin} - m\mathrm{e}^{\eta\ell_0}$$

The relationship between the above four arbitrary constants is essential to obtain the final solutions to the differential equations. This relationship can be extracted from Equation (3):

$$\begin{aligned} G_c C_c \frac{\mathrm{d}t_c}{\mathrm{d}\ell} &= G_h C_h \frac{\mathrm{d}t_h}{\mathrm{d}\ell} \\ G_c C_c \times y\eta \mathrm{e}^{\eta\ell} &= G_h C_h \times m\eta \mathrm{e}^{\eta\ell}. \\ m &= \frac{G_c C_c}{G_h C_h} y \end{aligned}$$

On the other hand,

$$\begin{aligned} G_c C_c \frac{\mathrm{d}t_c}{\mathrm{d}\ell} &= Ah(t_h - t_c) \\ G_c C_c y\eta \mathrm{e}^{\eta\ell} &= Ah\Big(m\mathrm{e}^{\eta\ell} + n - y\mathrm{e}^{\eta\ell} - t_{cin} + y\Big) \end{aligned}$$

Then, replace m with $\frac{G_c C_c}{G_h C_h} y$ to simplify the above equation:

$$\begin{aligned} y\eta \mathrm{e}^{\eta\ell} &= Ah\Big(\frac{1}{G_h C_h} - \frac{1}{G_c C_c}\Big) y\mathrm{e}^{\eta\ell} + Ah\frac{n + y - t_{cin}}{G_c C_c} \\ &= y\eta \mathrm{e}^{\eta\ell} + \frac{Ah}{G_c C_c}(n + y - t_{cin}) \end{aligned}$$

Clearly, the second term on the right-hand side of the simplified equation shall be zero, which means that

$$n = t_{cin} - y = x$$

Thus, it is proven that m is the product of $\frac{G_c C_c}{G_h C_h}$ and y, n is equal to x. The last step is observing the difference between the boundary conditions, Equation (7b) minus Equation (7a), and using the relations between m and y, n and x, to determine the final expressions of the four constants.

$$\begin{aligned} t_{hin} - t_{cin} &= m\mathrm{e}^{\eta\ell_0} - y + (n - x) \\ &= \frac{G_c C_c}{G_h C_h} y\mathrm{e}^{\eta\ell_0} - y \end{aligned}$$

In other words,

$$\begin{aligned} y &= \frac{G_h C_h}{G_c C_c} m = \frac{t_{hin} - t_{cin}}{\frac{G_c C_c}{G_h C_h}\mathrm{e}^{\eta\ell_0} - 1} \\ n = x &= t_{cin} - y = t_{cin} - \frac{t_{hin} - t_{cin}}{\frac{G_c C_c}{G_h C_h}\mathrm{e}^{\eta\ell_0} - 1} \end{aligned}$$

Thus far, the four arbitrary constants in Equation (5a,5b) have been confirmed, and the temperature distributions of the counterflow heat transfer process can be expressed as:

$$t_c = t_{cin} + \frac{\mathrm{e}^{\eta\ell} - 1}{\frac{G_c C_c}{G_h C_h}\mathrm{e}^{\eta\ell_0} - 1}(t_{hin} - t_{cin}) \tag{8a}$$

$$t_h = t_{hin} - \frac{\mathrm{e}^{-\eta(\ell_0 - \ell)} - 1}{\frac{G_h C_h}{G_c C_c}\mathrm{e}^{-\eta\ell_0} - 1}(t_{hin} - t_{cin}) \tag{8b}$$

It is clear that the temperature profiles are exponential functions that are determined by the inlet temperatures and heat capacity rates of both streams, as well as the thermal conductivity of the heat exchanger. For example, a counterflow heat exchanger is an essential element for recuperative cooling cycles, and the parameters of such a CFHX composed of shell and tubes in the reference [25] can be extracted and converted into the values as shown in Table 1. The working fluid of this CFHX is water and the specific heat capacity is chosen to be at constant volume. The temperature profiles are shown in Figure 2, produced using a MATLAB algorithm.

Table 1. Parameters of the demonstrated CFHX and its streams.

A $\mathrm{m^2}$	h $\mathrm{W/(m^2 \cdot K)}$	ℓ_0 m	G_h kg/s	G_c kg/s	C_v $\mathrm{J/(kg \cdot K)}$	t_{hin} K	t_{cin} K
1.81	20,000	1	4	2	4182	353	298

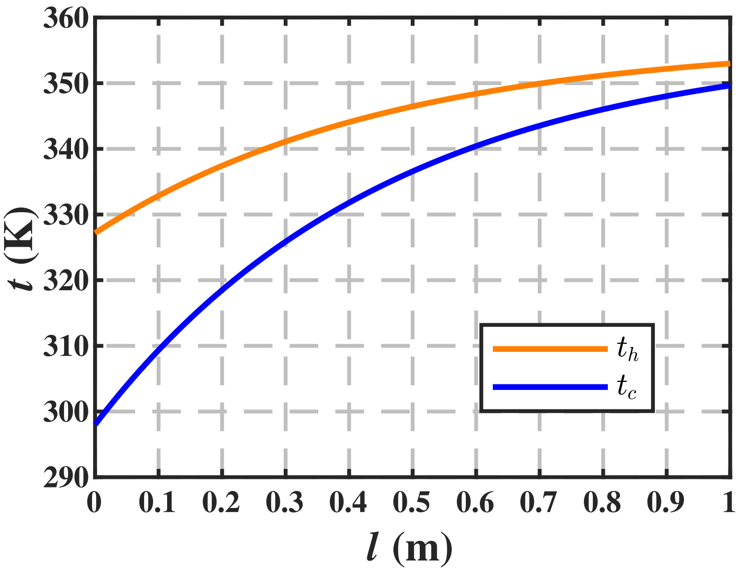

Figure 2. Temperature profiles of above demonstrated CFHX.

However, when the cold stream and the hot stream have the same heat capacity rates, the value of η is zero; thus, the numerator and denominator in Equation (8a,8b) tend to be zero, too. This renders the expressions of the above temperature profiles valueless. The mathematical solutions to the temperature distribution for this case are different; the heat capacity rate can be expressed as

$$G_c C_c = G_h C_h = GC$$

Equation (3) is converted to the following form:

$$\frac{\mathrm{d}t_c}{\mathrm{d}\ell} = \frac{\mathrm{d}t_h}{\mathrm{d}\ell} = \frac{Ah}{GC}(t_h - t_c) \tag{9}$$

and the derivative of the above differential equation is

$$\frac{\mathrm{d}^2 t_c}{\mathrm{d}\ell^2} = \frac{\mathrm{d}^2 t_h}{\mathrm{d}\ell^2} = \frac{Ah}{GC}\left(\frac{\mathrm{d}t_h}{\mathrm{d}\ell} - \frac{\mathrm{d}t_c}{\mathrm{d}\ell}\right) = 0$$

Thus,

$$\frac{\mathrm{d}t_h}{\mathrm{d}\ell} = \frac{\mathrm{d}t_c}{\mathrm{d}\ell} = m \tag{10}$$

where m is an arbitrary constant, and this means that the temperatures of both the cold and hot stream are linear functions related to ℓ:

$$t_c = m\ell + c_1$$
$$t_h = m\ell + c_2$$

where c_1 and c_2 are arbitrary constants, too. The boundary conditions are as follows: when ℓ is 0, the temperature of the hot stream is t_{hin}, and when ℓ equals ℓ_0, the temperature of the cold stream is t_{cin}.

$$t_c = c_1 = t_{cin} \tag{11a}$$
$$t_h = m\ell_0 + c_2 = t_{hin} \tag{11b}$$

From Equations (9) and (10), the following formula is obtained:

$$\frac{\mathrm{d}t_c}{\mathrm{d}\ell} = \frac{\mathrm{d}t_h}{\mathrm{d}\ell} = \frac{Ah}{GC}(t_h - t_c) = m$$

which means that

$$\frac{Ah}{GC}(c_2 - c_1) = m$$

We then use the information in the boundary conditions, Equation (11a,11b), to replace the arbitrary constants c_1, c_2 in the above formula. In other words,

$$t_{hin} - m\ell_0 - t_{cin} = \frac{GC}{Ah}m$$

From the above equation, it is easy to obtain the expression of m:

$$m = \frac{Ah(t_{hin} - t_{cin})}{GC + Ah\ell_0}$$

Thus,

$$c_1 = t_{cin}$$
$$c_2 = t_{hin} - m\ell_0 = t_{hin} - \frac{Ah\ell_0(t_{hin} - t_{cin})}{GC + Ah\ell_0}$$

and the temperature distributions of the hot and cold stream with the same heat capacity rate are solved.

$$t_c = t_{cin} + \frac{Ah\ell(t_{hin} - t_{cin})}{GC + Ah\ell_0} \tag{12a}$$
$$t_h = t_{hin} - \frac{Ah(\ell_0 - \ell)(t_{hin} - t_{cin})}{GC + Ah\ell_0} \tag{12b}$$

Thus far, the general solutions to the counterflow heat transfer process have been obtained. Equation (8a,8b) are the formulas for working conditions in which the heat capacity flow rates of the two streams are different; in this case, the temperature profiles are exponential functions, the derivative ratio of which is the inverse ratio of the heat capacity rates. Equation (12a,12b) show the temperature distributions of the heat exchanger with the same heat capacity flow rates, and in this case, the temperature profiles are linear functions with the same slope. The temperature curves are shown in Figure 3 for the case in which the mass flow rates of both streams of the above demonstrated CFHX are 4 kg/s.

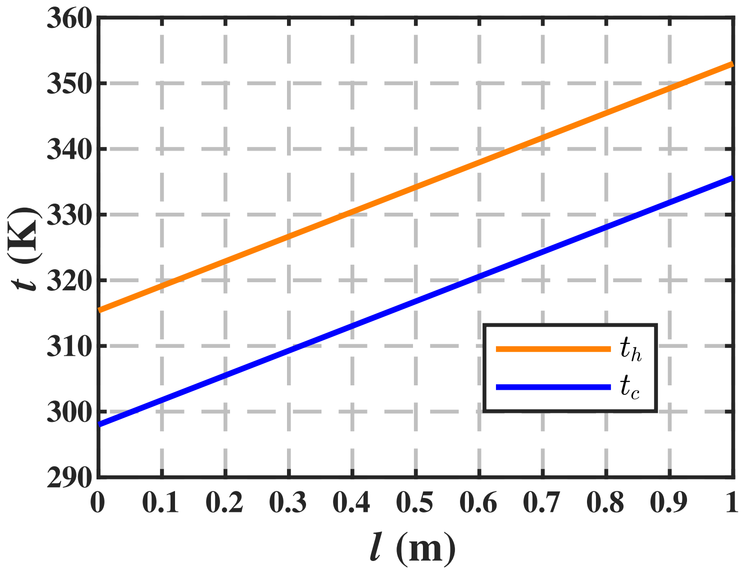

Figure 3. Temperature profiles of the demonstrated CFHX with same heat capacity rates.

3. Amount of Heat Transferred

Depending on the analytical expressions of the local temperatures, it is easy to obtain the amount of heat that an exchanger transfers. From Equation (8a,8b), the differential energy transferred from the hot stream to the cold stream in the finite volume shown in Figure 1 can be written as:

$$\begin{aligned}\delta Q &= Ah(t_h - t_c)\,\mathrm{d}\ell \\ &= Ah\frac{t_{hin} - t_{cin}}{e^{\eta\ell_0} - \frac{G_hC_h}{G_cC_c}}\left(1 - \frac{G_hC_h}{G_cC_c}\right)e^{\eta\ell}\,\mathrm{d}\ell\end{aligned}$$

and the total heat amount is the integration of the above differential energy:

$$\begin{aligned}Q &= Ah\frac{t_{hin} - t_{cin}}{e^{\eta\ell_0} - \frac{G_hC_h}{G_cC_c}}\left(1 - \frac{G_hC_h}{G_cC_c}\right)\int_0^{\ell_0} e^{\eta\ell}\,\mathrm{d}\ell \\ &= G_hC_hG_cC_c(t_{hin} - t_{cin})\frac{e^{\eta\ell_0} - 1}{G_cC_ce^{\eta\ell_0} - G_hC_h}\end{aligned}$$

Meanwhile, it can also be compared with the ε-NTU method; when G_cC_c is smaller than G_hC_h, Q is:

$$Q = G_cC_c(t_{hin} - t_{cin})\frac{1 - e^{\eta\ell_0}}{1 - \frac{G_cC_c}{G_hC_h}e^{\eta\ell_0}}$$

otherwise,

$$Q = G_hC_h(t_{hin} - t_{cin})\frac{1 - e^{-\eta\ell_0}}{1 - \frac{G_hC_h}{G_cC_c}e^{-\eta\ell_0}}$$

Then, we can define NTU and C_r as:

$$NTU = \frac{hA\ell_0}{(GC)_{min}} C_r = \frac{(GC)_{min}}{(GC)_{max}}$$

Hence,

$$Q = (GC)_{min}\varepsilon(t_{hin} - t_{cin})$$

where,

$$\varepsilon = \frac{1 - e^{-NTU(1-C_r)}}{1 - C_re^{-NTU(1-C_r)}}$$

When the hot and cold streams have the same heat capacity rate, the total amount of heat is obtained from Equation (12a,12b):

$$\begin{aligned} Q &= \int_0^{\ell_0} Ah(t_h - t_c)\,\mathrm{d}\ell \\ &= GC(t_{hin} - t_{cin})\frac{Ah\ell_0}{GC + Ah\ell_0} \end{aligned}$$

In this case,

$$\varepsilon = \frac{NTU}{1 + NTU}$$

The overall heat exchanged in a CFHX is obtained from local temperatures in this article, and the result is exactly the same as that derived by Prof. Bergman through the logarithmic mean temperature difference [13]. This proves that the mathematical expressions of the temperature profiles are correct, and these expressions make it convenient to analyze the features of a counterflow heat exchanger.

4. Features of Counterflow Heat Exchangers

The first feature of a counterflow heat transfer process is the rotational symmetry of the temperature profiles. When the hot and cold streams exchange their heat capacity rates, the temperature profiles are similar to before but rotate 180°, and the amount of overall heat transferred is the same. We can define the following:

$$\begin{aligned} G'_h C'_h &= G_c C_c \\ G'_c C'_c &= G_h C_h \end{aligned}$$

We keep all other parameters of the CFHX the same as before, such as the convection heat transfer coefficient and inlet temperatures; only the heat capacity flow rates of the two streams are exchanged with each other. The temperatures of the hot and cold streams are functions of ℓ, which can be expressed as:

$$t_h = f(\ell) \qquad t_c = g(\ell)$$

and

$$t'_h = q(\ell) \qquad t'_c = p(\ell)$$

It is easy to derive the following equation from the expressions of the temperature profiles:

$$q(\ell_0 - \ell) - p(\ell_0 - \ell) = f(\ell) - g(\ell) \tag{13}$$

This means that the temperature difference at ℓ in the CFHX with stream parameters, $G_h C_h$ and $G_c C_c$ is the same as the temperature difference at $(\ell_0 - \ell)$, where the stream parameters are $G'_h C'_h$ and $G'_c C'_c$. In order to clarify the conclusion, a CFHX with the parameter values in Table 1 is analyzed again after the mass flow rates are exchanged with each other as shown in Table 2.

Table 2. Mass flow rates of two symmetrical cases.

G_h kg/s	G_c kg/s	G'_h kg/s	G'_c kg/s	C_v J/(kg · K)
4	2	2	4	4182

The temperature profiles of t'_h and t'_c are given in Figure 4. They are exponential functions, the shape of which is different from that in Figure 2. When the heat capacity rate of the hot stream is higher than that of the cold stream, the temperature profiles are concave functions (Figure 2); otherwise, they are convex functions as shown in Figure 4.

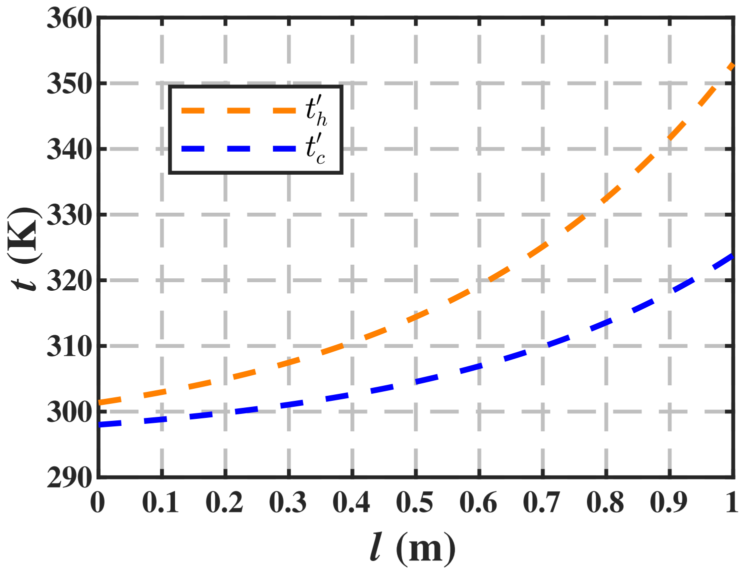

Figure 4. Temperature profiles of the above CFHX with exchanged heat capacity rates.

To clarify this feature, the curves are compared in Figure 5. The inlet temperatures of the hot and cold streams are marked as A and B, respectively. Equation (13) reveals that curves AA' and BB'' are rotationally symmetrical around the midpoint of AB, which is marked as o. Meanwhile, curves AA'' and BB' have similar symmetry. The total amount of heat transferred in the CFHX is the product of hA and the area enclosed by the high and low temperature curves; hence, the two pairs of heat capacity rates result in the same total heat exchanged.

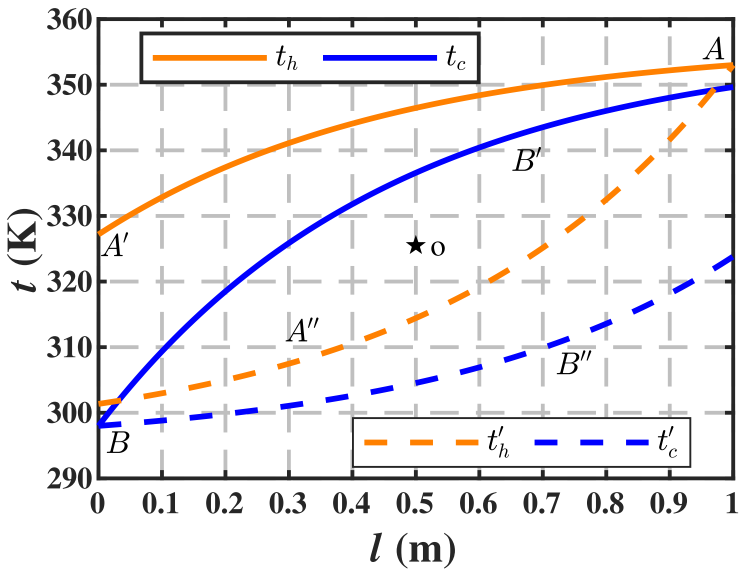

Figure 5. Temperature profiles of the demonstrated CFHX.

Next, in this section, we analyze the capability limit of a CFHX. Consider the hot and cold streams flowing through the heat exchanger with the same heat capacity rates:

$$G_hC_h = G_cC_c = GC$$

The following derivative equations can be obtained:

$$\frac{\mathrm{d}Q}{\mathrm{d}(GC)} = \frac{(Ah\ell_0)^2(t_{hin} - t_{cin})}{(Ah\ell_0 + GC)^2} > 0$$
$$\frac{\mathrm{d}^2Q}{\mathrm{d}(GC)^2} = -2\frac{(Ah\ell_0)^2(t_{hin} - t_{cin})}{(Ah\ell_0 + GC)^3} < 0$$

which reveals that the total amount of heat transferred increases at a slower rate when more fluids flow through the CFHX. As shown in Figure 6, when the heat capacity rate increases from zero to infinity, the total heat transferred increases from zero to its limit, $hA\ell_0(t_{hin} - t_{cin})$. When the fluid mass flow rate is less than 20 kg/s, the heat duty rapidly increases from 0, reaching 1.4×10^6 W, which is more than 70% of the heat duty limit. However, after $G > 20$ kg/s, the heat duty grows slowly, which shows that the performance of the CFHX will not be improved significantly when a great deal of mechanical energy is consumed. In reality, it is impossible to induce the fluids to flow through a CFHX with infinite mass flow rates, while, if there is condensation and evaporation happening in the heat exchanger, the equipment will work under two constant temperatures, and the total amount of heat transferred is the product of the thermal conductivity and the temperature difference.

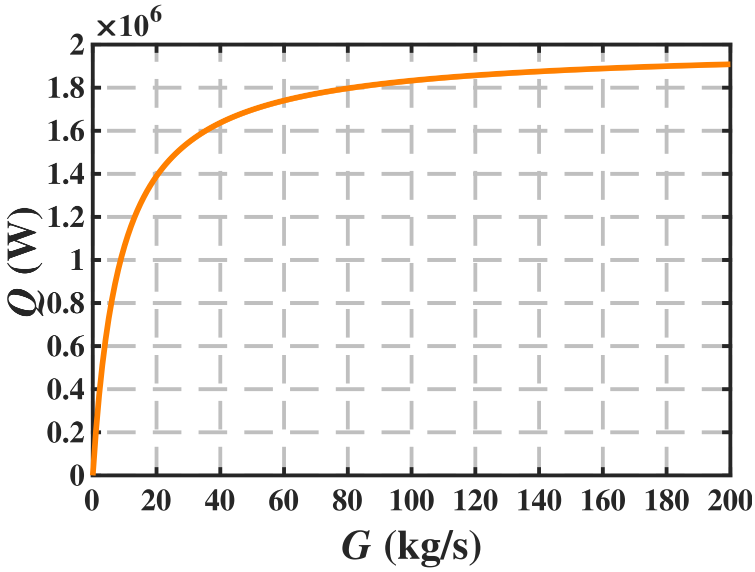

Figure 6. Capability limit of a CFHX.

The temperature profiles of the streams with different heat capacity rates are shown in Figure 7; they are linear functions, the slope of which becomes smaller with the increasing GC. In an ideal analysis, when the heat capacity rates increase to a value that is large enough, the temperature profile becomes a pair of horizontal lines, as shown in Figure 8. In a real process, when the condensation of the hot fluid (as gas) and evaporation of the cold fluid (as liquid) occur simultaneously in the CFHX, the latent heat of gas liquefaction on the hot side is transferred to the cold side and absorbed by the cold liquid. The heat energy is converted to the latent heat of vaporization and the CFHX operates under constant temperatures. Nevertheless, the total amount of heat transferred by the CFHX is between zero and the production of thermal conductivity and the inlet temperature difference.

$$Q \in \left(0, hA\ell_0(t_{hin} - t_{cin})\right)$$

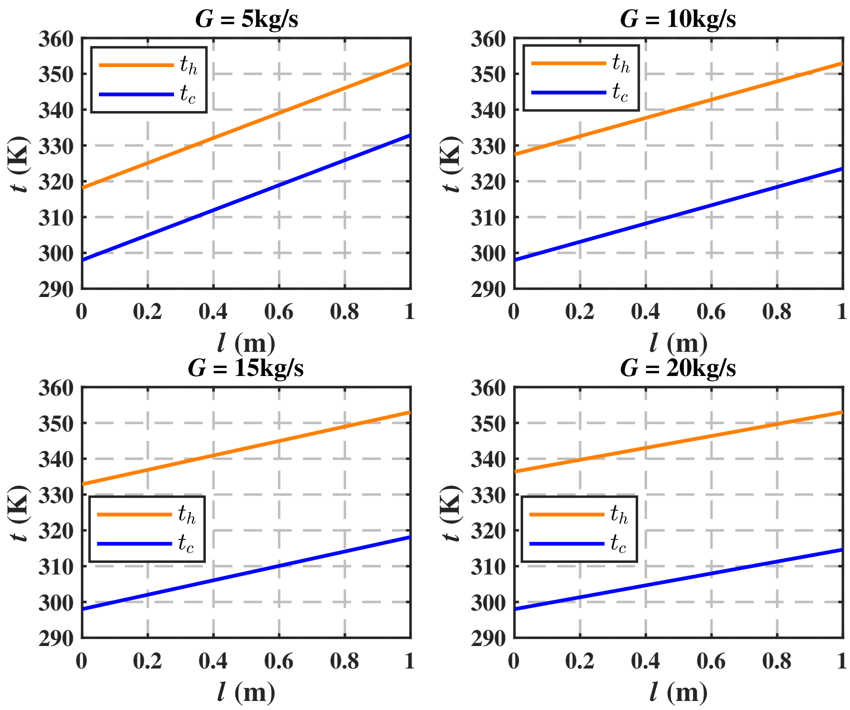

Figure 7. Temperature profiles of the streams with four pairs of heat capacity rates.

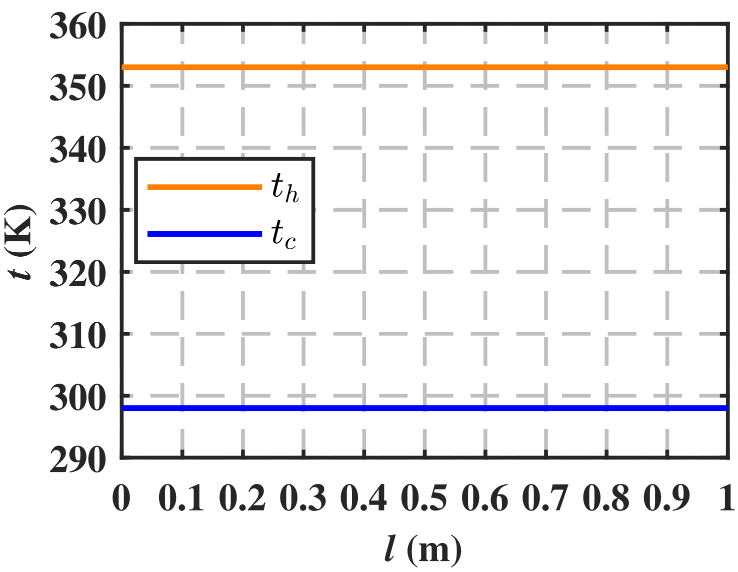

Figure 8. Temperature profiles of the streams with infinite heat capacity rates.

The third main aspect discussed in this section is the amount of heat exchanged in a CFHX under a certain level of mechanical energy consumption. The parameters are kept the same as before. In this case, the working fluids at both sides are liquid water, whose physical parameters are considered as same. Hence, the certain total mechanical energy consumption means that the corresponding total heat capacity rate is fixed and can be expressed as

$$2GC = G_h C_h + G_c C_h$$

where GC is the average heat capacity rate of the two streams. The percentage of the heat capacity rate of the hot stream can be defined as r,

$$\begin{aligned} G_h C_h &= 2rGC \\ G_c C_c &= 2(1-r)GC \end{aligned}$$

Thus, the total amount of heat transferred is

$$\begin{aligned} Q &= 2GC(t_{hin} - t_{cin}) \frac{r(1-r)\left(\mathrm{e}^{\eta \ell_0} - 1\right)}{(1-r)\mathrm{e}^{\eta \ell_0} - r} \\ \eta &= Ah\left(\frac{1}{2rGC} - \frac{1}{2(1-r)GC}\right) \end{aligned}$$

and the following first and second derivative can be obtained:

$$\begin{aligned} \left.\frac{\mathrm{d}Q}{\mathrm{d}r}\right|_{r=\frac{1}{2}} &= 0 \\ \frac{\mathrm{d}^2 Q}{\mathrm{d}r^2} &< 0 \end{aligned}$$

which indicates that the amount of heat transferred will reach its maximum value when the hot and cold fluids flow through the CFHX with the same mass flow rate, where $r = 0.5$, as shown in Figure 9. The total mass flow rate is 10 kg/s and the temperature profiles for four pairs of mass flow rates are depicted in Figure 10. The total amount of heat transferred is the product of the thermal conductivity hA and the area enclosed by the temperature curves. It is clearly shown in Figure 10 that this area becomes increasingly large when r increases from 0 to 0.5; then, the area decreases in a symmetrical way.

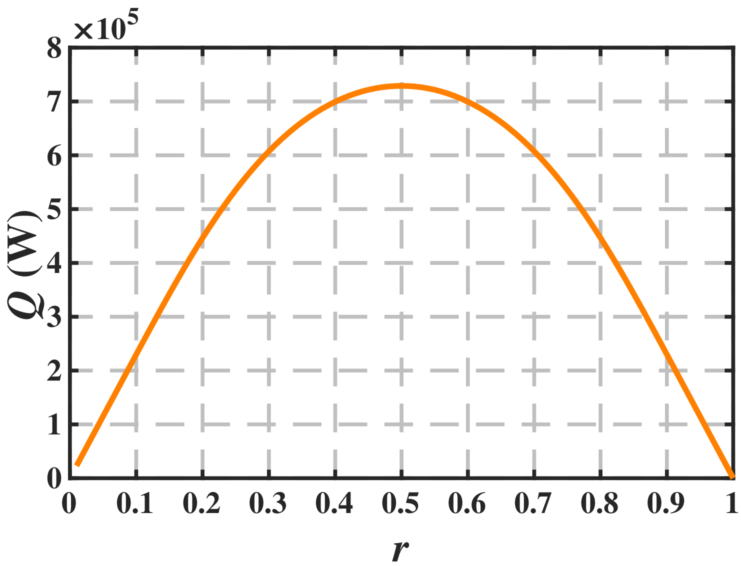

Figure 9. The amount of heat transferred under certain mechanical energy consumption.

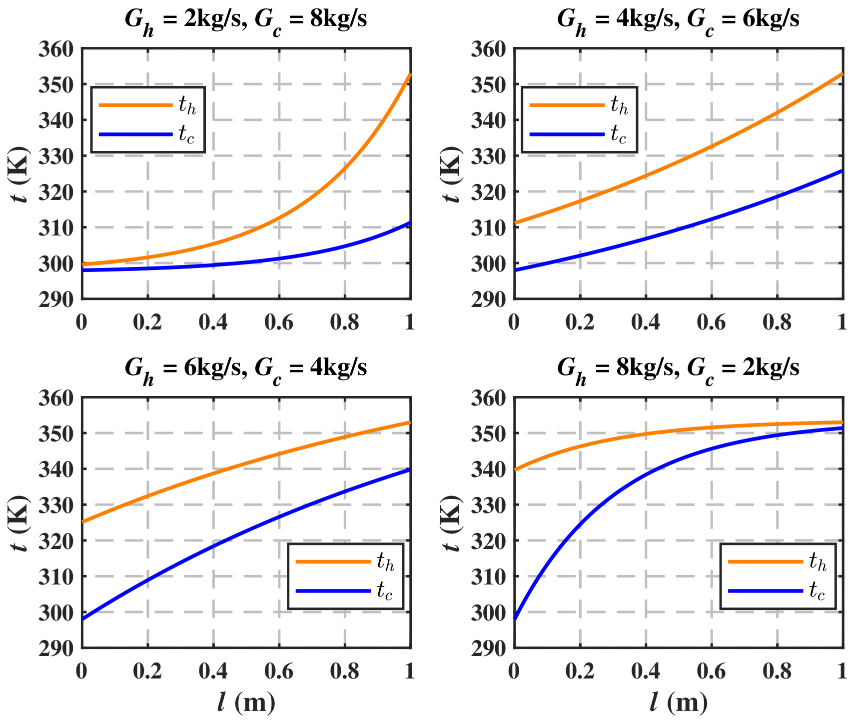

Figure 10. Temperature profiles for four pairs of mass flow rates.

5. Distribution of Entropy Generation

Entropy generation is an important criterion to evaluate the irreversibility of the heat transfer process and it relies on two simultaneous sources: heat transfer between two streams with different temperatures, and the existence of a pressure drop due to the imposed resistance to flow. Both the flow character and heat transfer will be calculated in the design of a heat exchanger, but the two sources of entropy generation are different and there is no useful method to compare them in an ideal heat transfer process. In the design of a heat exchanger, different loss mechanisms such as pressure drop and parasitic heat flows are often treated separately. Pressure drop caused by flow resistance is determined by the real structure of the heat exchanger and the flow rates of the fluids; it is difficult to evaluate the amount of this mechanical energy consumption in mathematical analyses. This paper only reveals the features of the balanced heat transfer process, ignoring the pumping or blowing mechanical energy consumption. Thus, only the entropy generation contributed by heat transfer will be analyzed after the temperature profiles are derived from the differential equations.

In the past, total entropy generation was evaluated to optimize the design of heat exchangers. The ε-NTU method does not provide any analysis of the local distribution of entropy generation. Meanwhile, in this paper, as with the local temperatures, the local distribution of entropy generation is considered, too. Firstly, differential and total entropy generation are, respectively, written as:

$$\delta S_g = G_c C_c \frac{\mathrm{d}t_c}{t_c} - G_h C_h \frac{\mathrm{d}t_h}{t_h}$$

$$\begin{aligned} S_g &= G_c C_c \int_{t_{cin}}^{t_{cout}} \frac{1}{t_c}\,\mathrm{d}t_c - G_h C_h \int_{t_{hout}}^{t_{hin}} \frac{1}{t_h}\,\mathrm{d}t_h \\ &= G_c C_c \ln \frac{t_{cout}}{t_{cin}} + G_h C_h \ln \frac{t_{hout}}{t_{hin}} \end{aligned}$$

and it is useful to analyze the relationship between entropy generation and stream temperatures:

$$\begin{aligned}\delta S_g &= \delta Q\Big(\frac{1}{t_c} - \frac{1}{t_h}\Big) \\ &= hA\,\mathrm{d}\ell(t_h - t_c)\Big(\frac{1}{t_c} - \frac{1}{t_h}\Big) \\ &= hA\,\mathrm{d}\ell\Big(\frac{t_h}{t_c} + \frac{1}{\frac{t_h}{t_c}} - 2\Big)\end{aligned}$$

Clearly, the entropy generation is determined by the ratio of the hot stream temperature to the cold one. The above expression is a kind of hook function, and local entropy generation is proven to be a relevant variable for local temperatures, the ratio of which is marked as x,

$$f(x) = x + \frac{1}{x} \quad x \in (0, +\infty)$$

An image of the above hook function is shown in Figure 11. The lines, $x = 0$ and $y = x$, are two asymptotes of the hook function. When x belongs to interval $(0, 1)$, $f(x)$ is a decreasing function; it increases with x when the independent variable is larger than 1.

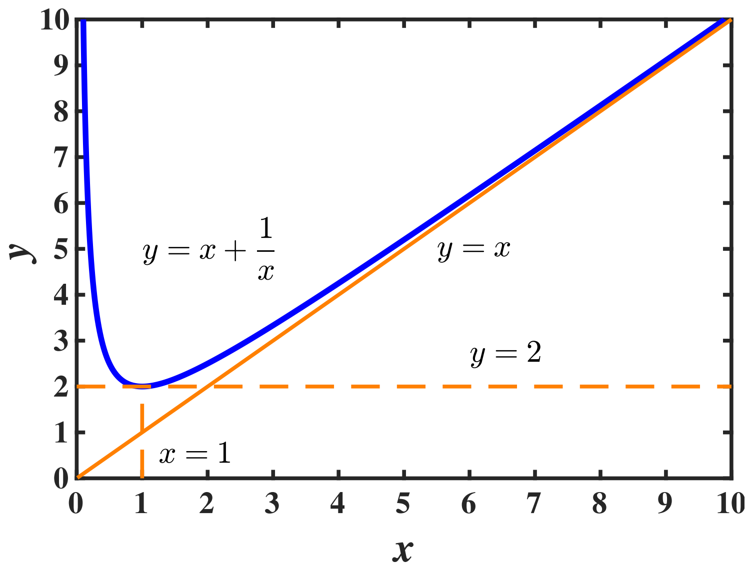

Figure 11. The curve of the typical hook function.

In a heat exchanger, the ratio of hot to cold stream temperature is always larger than 1. This means that the local entropy generation is a monotonically increasing function of the local temperature ratio.

As a fourth-generation nuclear reactor, a high-temperature gas-cooled reactor (HTGR) has distinct advantages in terms of inherent safety, economic potential, high efficiency, etc. A HTGR can conceptually have a outlet temperature of 1000 °C and, in the actual working process, this temperature can reach around 770 °C. The helical steam generator of the HTGR is a kind of counterflow heat exchanger, the main parameters of which are extracted in Table 3. The fluid of the hot stream is helium, whose mass flow rate is 4.32 kg/s under normal working conditions. The cold stream is water vapor with a mass flow rate of 3.29 kg/s. The average heat capacities at the same pressure and inlet temperatures of the two streams are simplified as shown in Table 3 [26].

Table 3. Parameters of the helical steam generator of HTGR.

A $\mathbf{m}^2$	h $\mathbf{W/(m^2 \cdot K)}$	ℓ_0 $\mathbf{m}$	C_{ph} $\mathbf{J/(kg \cdot K)}$	C_{pc} $\mathbf{J/(kg \cdot K)}$	t_{hin} $\mathbf{K}$	t_{cin} $\mathbf{K}$
10	1500	4	5190	4530	1043	373

This paper investigates the temperature profiles of streams working under normal conditions, as well as the temperature profiles when the heat capacity rates are exchanged with each other, whose values are shown in Table 4. As seen in Figure 12, the temperature curves are concave functions when the heat capacity rate of the hot stream is higher than that of the cold stream; otherwise, they are convex functions. Nevertheless, the curves have the feature of rotational symmetry, as depicted previously, and the areas enclosed by them are equivalent so that the heat exchanged in the two cases is the same: Q = 9,267,255.59 W.

Table 4. Heat capacity rates of the streams in the helical steam generator studied.

$G_h C_{ph}$ **W/K**	$G_c C_{pc}$ **W/K**	$G'_h C_{ph}$ **W/K**	$G'_c C_{pc}$ **W/K**
22,420.8	15,809.7	15,809.7	22,420.8

It is interesting to analyze the local entropy generation in the helical steam generator. Its distribution is determined by the ratio of high to low temperature in the form of the hook function. It is clearly illustrated in Figure 12 that the largest and smallest value of local entropy generation occur in the case under normal working conditions, and the inverse case gives a moderate and nearly uniform entropy generation distribution, the locations of which on a hook function are shown in Figure 13. The dimensionless local entropy generation rate of the steam generator working under normal conditions ranges from AA to BB, while in the other case, it ranges from $A'A'$ to $B'B'$. In contrast to the local heat transfer rates, the local entropy generation rates are not symmetrical and the total entropy generation has different values: $S_{gen} = 3617.19$ W/K, $S'_{gen} = 3669.67$ W/K.

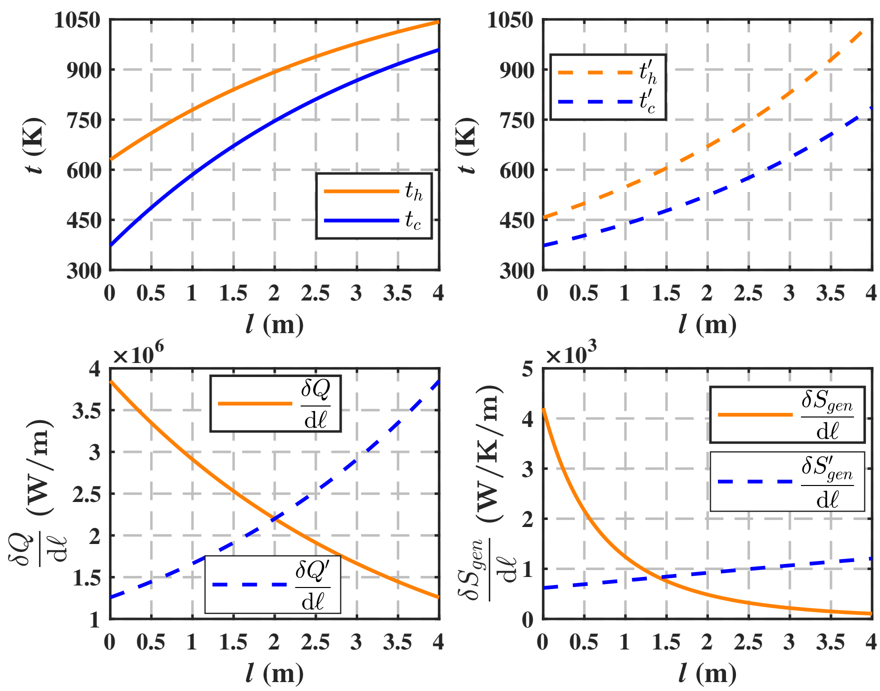

Figure 12. Temperature profiles, local heat transfer rates and entropy generation rates in the helical steam generator.

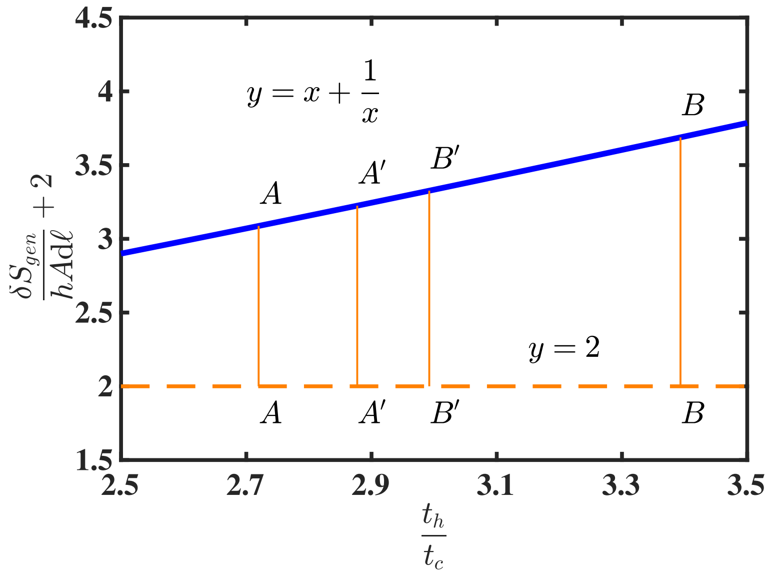

Figure 13. The ranges of the dimensionless entropy generation distribution of two cases in the hook function.

The "entropy generation paradox" could be explained through the local entropy generation rate. Heat exchanger effectiveness ε can be maximum, intermediate or minimum at the maximum irreversibility operation point depending on the flow arrangement of the two streams, and the ε-*NTU* method cannot explain this phenomenon. In this paper, we address this problem: if the heat capacity rates of the hot and cold streams are exchanged with each other, the equipment realizes the same heat duty with the same effectiveness ε, but the profiles of the local entropy generation rates are different, resulting in different total entropy generation. This is the reason for the discrepancy between the effectiveness and irreversibility.

To achieve this certain amount of heat exchanged, $Q = 9{,}267{,}255.59$ W, there are an infinite variety of heat capacity rate couples to choose. For example, Figure 14 shows different temperature profiles for four pairs of heat capacity rate arrangements, all of which will result in the above total amount of heat transferred. The flow character is ignored and only the entropy generation caused by heat flux is calculated. The local entropy generation rates of the four demonstrated cases are shown in Figure 15. Clearly, each case has a unique local entropy generation profile and their total entropy generation values are shown in Table 5.

It is clear that there is a specific pair of heat capacity rates that causes the minimum total entropy generation, in order to realize the above amount of heat transferred. Different heat capacity rate pairs and the corresponding total entropy generation values are shown in Figure 16. The best pair is marked by a red star and the heat capacity rates of both streams, as well as the total entropy generation, are shown in Table 6. The temperature profiles and local entropy generation of this best case are shown in Figures 17 and 18, respectively.

Table 5. Heat capacity rates of the streams and respective total entropy generation.

G_h kg/s	$G_h C_{ph}$ W/K	G_c kg/s	$G_c C_{pc}$ W/K	S_{gen} W/K
3.464	17,978.16	3.968	17,975.04	3348.40
8.64	44,841.6	3.185	14,428.05	4549.75
12.96	67,262.4	3.144	14,242.32	4854.84
∞	∞	3.096	14,024.88	5420.87

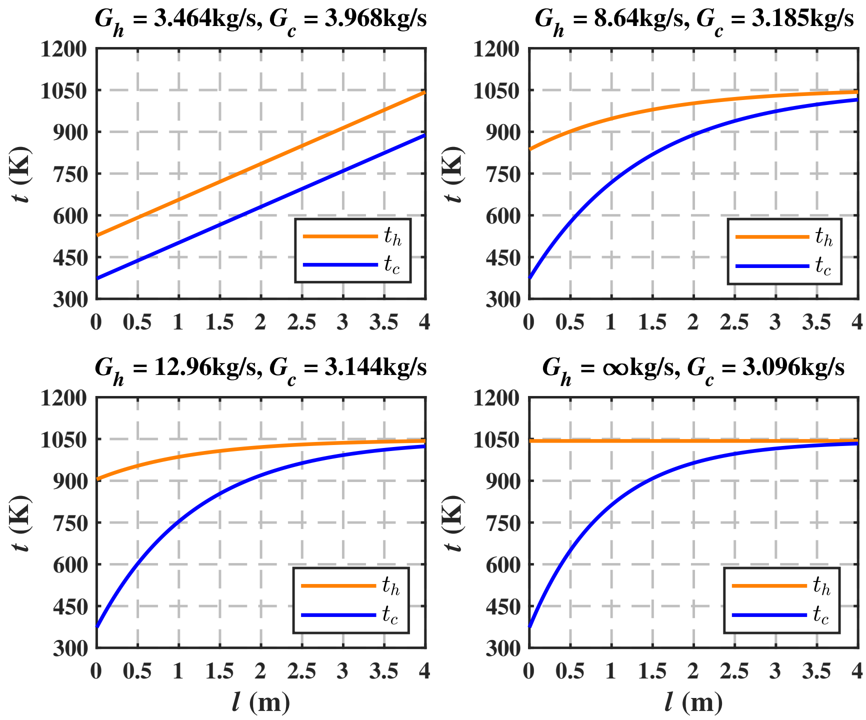

Figure 14. Four pairs of heat capacity rates to realize a specific amount of heat transfer.

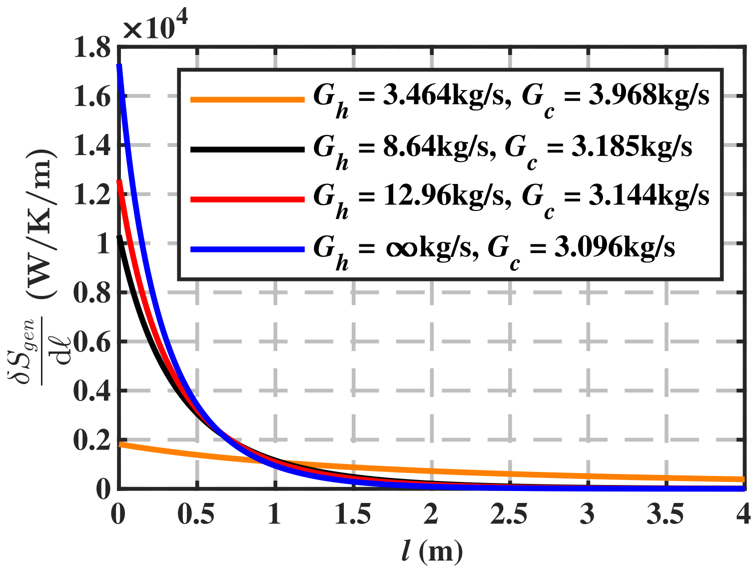

Figure 15. Local entropy generation rates of the four demonstrated cases.

Table 6. Heat capacity rates of the streams and respective total entropy generation for the best case.

G_h kg/s	G_hC_{ph} W/K	G_c kg/s	G_cC_{pc} W/K	S_{gen} W/K
3.4408	17,857.97	3.9948	18,096.62	3346.83

Tondeur revealed that, in a contacting or separation device involving a given transfer area and achieving a specified transfer duty, the total entropy generation is minimal when the local rate of entropy generation is uniformly distributed (equipartitioned) along the space and/or time variables [27]. The principle was confirmed again by Johannessen, and the theoretical result can be used as an argument that the heat exchange process is characterized by a constant local entropy generation rate that gives the best second law efficiency possible. The optimal heat exchange conditions are therefore well approximated in practice with a counterflow heat exchanger with an approximately constant temperature difference between the fluids [28].

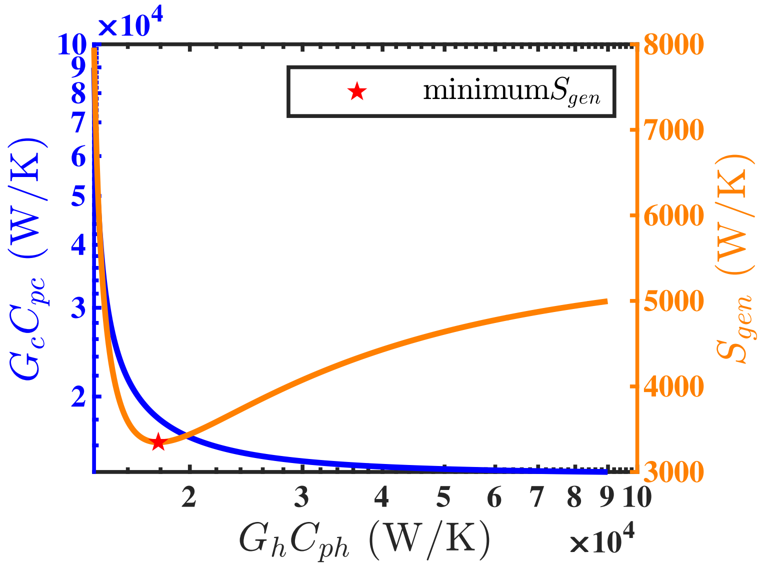

Figure 16. Different heat capacity rate pairs and corresponding total entropy generation.

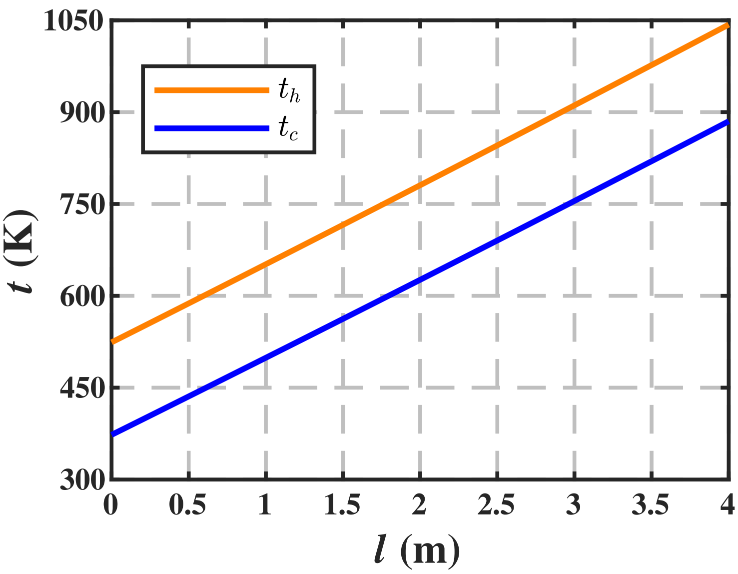

Figure 17. The temperature profiles of the case with the minimum total entropy generation.

In a real heat exchanger, there is no way to determine a certain pair of heat capacity rates to make the local distribution of entropy generation rate truly uniform. In fact, the above pair does not exist. In spite of this reality, the optimal case working under minimum total irreversibility can be obtained, and it is easy to find that the local rate of entropy generation is relatively uniform compared with other cases, as shown in Figure 15. The orange curve, which represents $G_h = 3.464$ kg/s and $G_c = 3.968$ kg/s, shows a much more uniform distribution of the local entropy generation compared with the other three cases. The optimal distribution is shown in Figure 18 and the value range of this best case is close to the orange curve in Figure 15. The deviation of total entropy generation of the two cases is less than 0.047% and the above principle is confirmed: the equipartition of entropy generation is an optimal criterion for heat transfer processes. The counterflow heat exchanger performs better than the parallel flow heat exchanger; this can be explained by the fact that the CFHX could operate under a nearly uniform local entropy generation rate, while the distribution of the entropy generation rate of the PFHX presented a considerable difference between the inlet and outlet position when the equipment attempted to achieve the same heat duty. The parallel flow heat exchanger performs with lower efficiency and results in a higher economic cost.

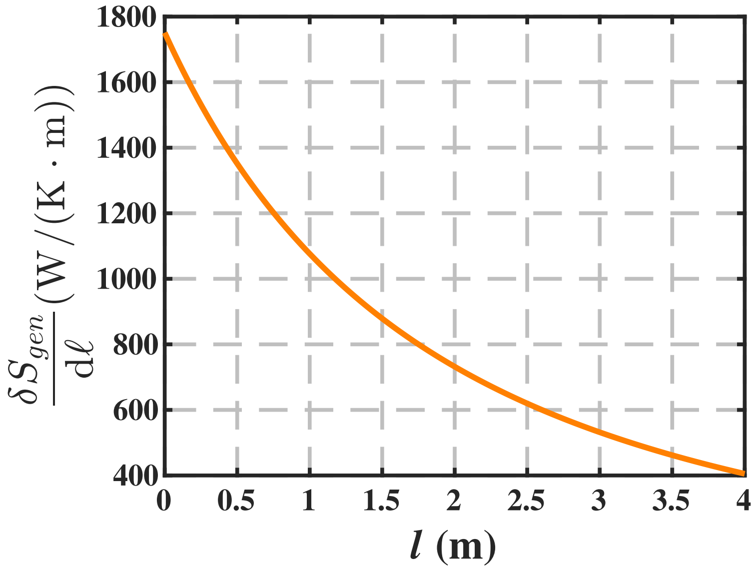

Figure 18. The local entropy generation profile of the above best case.

Less total entropy generation means a greater economic benefit. When the high-temperature gas-cooled reactor works under this best pair of heat capacity rates, it will export the maximum mechanical energy and produce the most electricity [16].

6. Summary

This paper conducts a theoretical analysis of the local distribution of temperatures and entropy generation rates in an ideal counterflow heat exchanger. The mathematical solutions to the temperature profiles are obtained.

A heat exchanger is used to illustrate the features of temperature profiles: when the heat capacity rate of the hot stream is higher than that of the cold one, the temperature curves are concave exponential functions; otherwise, they are convex exponential functions. The derivative ratio of the temperature curves is equal to the inverse ratio of the heat capacity rates of the respective streams. If the hot and cold fluids flow through the heat exchanger with the same heat capacity rate, the temperature profiles are linear functions with the same slope. The demonstrated counterflow heat exchanger also illustrates the rotational symmetry feature of the CFHX: when the heat capacity rates of the hot and cold stream are exchanged with each other, the temperature profiles have rotational symmetry and the heat exchanger realizes the same heat duty.

Local entropy generation is determined by the ratio of the temperature of the hot stream to that of the cold stream, in the form of a hook function. The helical steam generator of a high-temperature gas-cooled reactor is a kind of counterflow heat exchanger, and the local entropy generation of a helical steam generator is analyzed in this article. The "entropy generation paradox" could be explained through the local entropy generation rate: if the heat capacity rates of the hot and cold streams are exchanged with each other, the equipment realizes the same heat duty with the same effectiveness ε, but the profiles of the local entropy generation rates are different, resulting in different total entropy generation. In order to achieve specific heat duty, there are infinite pairs of heat capacity rates. Each pair gives a unique local entropy generation profile, and the optimal case working under minimum total irreversibility is characterized by a nearly uniform local entropy generation distribution. This principle has been called the Equipartition of Entropy Generation by researchers, and it is proven to be accurate in this paper and shall be used to guide the design of heat transfer equipment.

Author Contributions: Z.D.: directed the research and wrote the paper; Q.D.: helped to complete the research. All authors have read and agreed to the published version of the manuscript.

Funding: This document is the result of a research project funded by the National Natural Science Foundation of China (No. 51736004 and No. 51776079).

Institutional Review Board Statement: Not applicable.

Informed Consent Statement: Not applicable.

Conflicts of Interest: The authors declare no conflict of interest.

Nomenclature

variables

A	Heat transfer area per unit length (m)
C	Specific heat capacity (J/(kg·K))
G	Mass flow rate (kg/s)
h	Convection heat transfer coefficient (W/(m^2·K)
Q	Heat transfer duty (W)
S_{gen}	Entropy generation (W/K)
t	Temperature (K)

subscripts

in	Inlet parameter
out	Outlet parameter
c	Cold stream
h	Hot stream
p	At constant pressure
v	At constant volume

References

1. Abbasian Arani, A.A.; Moradi, R. Shell and tube heat exchanger optimization using new baffle and tube configuration. *Appl. Therm. Eng.* **2019**, *157*, 113736. [CrossRef]
2. Chekurov, S.; Kajaste, J.; Saari, K.; Kauranne, H.; Pietola, M.; Partanen, J. Additively manufactured high-performance counterflow heat exchanger. *Prog. Addit. Manuf.* **2019**, *4*, 55–61. [CrossRef]
3. Kalapala, L.; Devanuri, J.K. Influence of operational and design parameters on the performance of a PCM based heat exchanger for thermal energy storage—A review. *J. Energy Storage* **2018**, *20*, 497–519. [CrossRef]
4. Sheikholeslami, M.; Haq, R.; Shafee, A.; Li, Z.; Elaraki, Y.G.; Tlili, I. Heat transfer simulation of heat storage unit with nanoparticles and fins through a heat exchanger. *Int. J. Heat Mass Transf.* **2019**, *135*, 470–478. [CrossRef]
5. El-Said, E.M.S.; Abou Al-Sood, M.M. Shell and tube heat exchanger with new segmental baffles configurations: A comparative experimental investigation. *Appl. Therm. Eng.* **2019**, *150*, 803–810. [CrossRef]
6. Zhang, X.; Liu, Z.; Liu, W. Numerical studies on heat transfer and friction factor characteristics of a tube fitted with helical screw-tape without core-rod inserts. *Int. J. Heat Mass Transf.* **2013**, *60*, 490–498. [CrossRef]
7. Liu, W.; Liu, Z.; Guo, Z. Physical quantity synergy in laminar flow field of convective heat transfer and analysis of heat transfer enhancement. *Chin. Sci. Bull.* **2009**, *54*, 3579–3586. [CrossRef]
8. Liu, W.; Liu, Z.; Ma, L. Application of a multi-field synergy principle in the performance evaluation of convective heat transfer enhancement in a tube. *Chin. Sci. Bull.* **2012**, *57*, 1600–1607. [CrossRef]
9. Liu, W.; Liu, P.; Dong, Z.M.; Yang, K.; Liu, Z.C. A study on the multi-field synergy principle of convective heat and mass transfer enhancement. *Int. J. Heat Mass Transf.* **2019**, *134*, 722–734. [CrossRef]
10. Liu, W.; Liu, P.; Wang, J.B.; Zheng, N.B.; Liu, Z.C. Exergy destruction minimization: A principle to convective heat transfer enhancement. *Int. J. Heat Mass Transf.* **2018**, *122*, 11–21. [CrossRef]
11. Zheng, N.; Yan, F.; Zhang, K.; Zhou, T.; Sun, Z. A review on single-phase convective heat transfer enhancement based on multi-longitudinal vortices in heat exchanger tubes. *Appl. Therm. Eng.* **2020**, *164*, 114475. [CrossRef]
12. Abeykoon, C. Compact heat exchangers—Design and optimization with CFD. *Int. J. Heat Mass Transf.* **2020**, *146*, 118766. [CrossRef]

13. Bergman, T.L.; Lavine, A.; Incropera, F.P.; Dewitt, D.P. *Fundamentals of Heat and Mass Transfer*; John Wiley & Sons: New York, NY, USA, 2017.
14. Alimoradi, A. Study of thermal effectiveness and its relation with NTU in shell and helically coiled tube heat exchangers. *Case Stud. Therm. Eng.* **2017**, *9*. [CrossRef]
15. Bejan, A. *Advanced Engineering Thermodynamics*; John Wiley & Sons: New York, NY, USA, 2016.
16. Bejan, A. Entropy generation minimization: The new thermodynamics of finite-size devices and finite-time processes. *J. Appl. Phys.* **1996**, *79*, 1191–1218. [CrossRef]
17. Nummedal, L.; Kjelstrup, S. Equipartition of forces as a lower bound on the entropy production in heat exchange. *Int. J. Heat Mass Transf.* **2001**, *44*, 2827–2833. [CrossRef]
18. Sheikholeslami, M.; Jafaryar, M.; Shafee, A.; Li, Z. Nanofluid heat transfer and entropy generation through a heat exchanger considering a new turbulator and CuO nanoparticles. *J. Therm. Anal. Calorim.* **2018**, *134*, 2295–2303.. [CrossRef]
19. Li, Z.; Sheikholeslami, M.; Jafaryar, M.; Shafee, A.; Chamkha, A.J. Investigation of nanofluid entropy generation in a heat exchanger with helical twisted tapes. *J. Mol. Liq.* **2018**, *266*, 797–805. [CrossRef]
20. Al-Rashed, A.A.; Ranjbarzadeh, R.; Aghakhani, S.; Soltanimehr, M.; Afrand, M.; Nguyen, T.K. Entropy generation of boehmite alumina nanofluid flow through a minichannel heat exchanger considering nanoparticle shape effect. *Phys. A Stat. Mech. Appl.* **2019**, *521*, 724–736. [CrossRef]
21. Lerou, P.P.P.M.; Veenstra, T.T.; Burger, J.F.; ter Brake, H.J.M.; Rogalla, H. Optimization of counterflow heat exchanger geometry through minimization of entropy generation. *Cryogenics* **2005**, *45*, 659–669. [CrossRef]
22. Mohamed, H.A. Entropy Generation in Counter Flow Gas to Gas Heat Exchangers. *J. Heat Transf.* **2005**, *128*, 87–92. [CrossRef]
23. Shah, R.K.; Skiepko, T. Entropy Generation Extrema and Their Relationship with Heat Exchanger Effectiveness—Number of Transfer Unit Behavior for Complex Flow Arrangements. *J. Heat Transf.* **2005**, *126*, 994–1002. [CrossRef]
24. Rauch, M.; Galović, A.; Ferdelji, N.; Mudrinić, S. Local Entropy Production of the Parallel Flow and Counterflow Heat Exchanger. *Trans. FAMENA* **2018**, *42*, 13–25. [CrossRef]
25. Wang, X.; Zheng, N.; Liu, Z.; Liu, W. Numerical analysis and optimization study on shell-side performances of a shell and tube heat exchanger with staggered baffles. *Int. J. Heat Mass Transf.* **2018**, *124*, 247–259. [CrossRef]
26. Ju, H.; Huang, Z.; Xu, Y.; Duan, B.; Yu, Y. Hydraulic Performance of Small Bending Radius Helical Coil-Pipe. *J. Nucl. Sci. Technol.* **2001**, *38*, 826–831. [CrossRef]
27. Tondeur, D.; Kvaalen, E. Equipartition of entropy production. An optimality criterion for transfer and separation processes. *Ind. Eng. Chem. Res.* **1987**, *26*, 50–56. [CrossRef]
28. Johannessen, E.; Nummedal, L.; Kjelstrup, S. Minimizing the entropy production in heat exchange. *Int. J. Heat Mass Transf.* **2002**, *45*, 2649–2654. [CrossRef]